



# Associated production of a dilepton and a $\Upsilon(J/\psi)$ at the LHC as a probe of gluon transverse momentum dependent distributions

Jean-Philippe Lansberg<sup>a</sup>, Cristian Pisano<sup>b,c</sup>, Marc Schlegel<sup>d,\*</sup>

<sup>a</sup> *IPNO, CNRS/IN2P3, Univ. Paris-Sud, Université Paris-Saclay, 91406 Orsay, France*

<sup>b</sup> *Dipartimento di Fisica, Università di Pavia, via Bassi 6, I-27100 Pavia, Italy*

<sup>c</sup> *INFN Sezione di Pavia, via Bassi 6, I-27100 Pavia, Italy*

<sup>d</sup> *Institute for Theoretical Physics, Universität Tübingen, Auf der Morgenstelle 14, D-72076 Tübingen, Germany*

Received 3 February 2017; received in revised form 3 April 2017; accepted 12 April 2017

Available online 18 April 2017

Editor: Hong-Jian He

## Abstract

We discuss the impact on the study of gluon transverse momentum dependent distributions (TMDs) of the associated production of a lepton pair and a  $\Upsilon$  (or a  $J/\psi$ ) in unpolarised proton–proton collisions,  $pp \rightarrow Q\ell\bar{\ell}X$ , at LHC energies, where one can assume that such final states are dominantly induced by gluon fusion. If the transverse momentum of the quarkonium–dilepton system – namely, the transverse momentum imbalance of the quarkonium state and the lepton pair – is small, the corresponding cross sections can be calculated within the framework of TMD factorisation. Using the helicity formalism, we show in detail how these cross sections are connected to the moments of two independent TMDs: the distribution of unpolarised gluons,  $f_1^g$ , and the distribution of linearly polarised gluons,  $h_1^{\perp g}$ . We complete our exhaustive derivation of these general relations with a phenomenological analysis of the feasibility of the TMD extraction, as well as some outlooks.

© 2017 The Author(s). Published by Elsevier B.V. This is an open access article under the CC BY license (<http://creativecommons.org/licenses/by/4.0/>). Funded by SCOAP<sup>3</sup>.

\* Corresponding author.

E-mail address: [marc.schlegel@uni-tuebingen.de](mailto:marc.schlegel@uni-tuebingen.de) (M. Schlegel).

## 1. Introduction

Three-dimensional momentum distributions of gluons in the nucleon – the so-called gluon transverse momentum dependent distributions (TMDs) – have attracted much attention recently [1,2]. Theoretically, gluon TMDs appear in factorisation formulae that explicitly take the transverse momentum of gluons into account (TMD factorisation), see *e.g.* [3–6]. These formulae apply to cross sections that are differential in the transverse momentum of the final state,  $\mathbf{q}_T$ , in a kinematical region where it is much smaller than the hard scale of the process  $Q$ ,  $|\mathbf{q}_T| \ll Q$ . Typically, the hard scale refers to the virtuality of the exchanged gauge boson in lepton–nucleon collisions or the invariant mass of the final state in hadron–hadron collisions. Our understanding of the evolution with the hard scale of the gluon TMDs has recently significantly improved, see *e.g.* [7–10].

Several processes have been identified as sensitive probes of gluon TMDs. Probably, the theoretically cleanest one is the production of a pair of (almost) back-to-back heavy quark and antiquark or of a di-jet in lepton–nucleon collisions [11–13]. A measurement of such processes could however only be performed at a future Electron–Ion–Collider. On the other hand, reactions initiated by two protons can also provide insights on the gluon TMDs at the LHC or at RHIC. For instance, one possibility is to look at di-photon production, still with a large azimuthal separation [14]. This process, however, suffers from additional contributions from quark-induced channels, at RHIC energies in particular. As such, it is probably not the cleanest probe of gluon TMDs in hadron collisions that one could think of. Furthermore, the experimental detection of direct photons requires a specific isolation procedure which may be difficult to implement in a realistic measurement.

A handier probe of gluon TMDs is certainly to be found among the production of quarkonium states [15–21], built up of either charm or bottom quarks, since they are often dominantly produced through gluon fusion at proton–proton colliders and some of them, like the spin triplet vector states, are relatively easy to detect in their di-muons channels. As for now, the access to gluon TMDs has been investigated in [15,6] with single inclusive  $\eta_{c,b}$  or  $\chi_{c,b}$ -production in proton collisions. One drawback of such single-particle analyses is that they are restricted to low transverse momenta, typically below half the quarkonium mass, which makes such experimental studies particularly challenging. Furthermore, in the case of  $\chi_{c,b}$ -production [22], TMD factorisation may not hold because of infrared divergences specific to the  $P$ -wave production.<sup>1</sup> Such issues do not appear for spin singlet  $S$ -wave state production, which however has so far only been studied for the  $\eta_c$  down to  $P_T \simeq 6$  GeV by the LHCb Collaboration [26].

This restriction on the usable phase space for TMD factorisation to apply can be avoided by looking at two-particle final states. One example is the associated production of a  $J/\psi$  or a  $\Upsilon$  with a direct photon [27]. Like for heavy-quark pair and di-jet electroproduction or di-photon hadroproduction, the large scale  $Q$  is set by the invariant mass of the system, which can be large when both the quarkonium and the photon are produced almost back to back with large individual transverse momentum, yet with a small transverse momentum for the pair (its imbalance). This is a rather convenient configuration to be studied experimentally. Moreover, in the case of quarkonium + photon production [27], one can enrich the event sample in colour-singlet contributions, which are purely from gluonic interaction, by isolating the quarkonium, since it has a non-zero transverse momentum. This makes it a golden-plated probe to extract gluon TMDs

<sup>1</sup> For reviews, the reader is referred to [23–25].

inside unpolarised protons at the LHC. However, along the lines of [28], it may be that colour-octet contributions to quarkonium production associated with a colour singlet particle, like a SM boson ( $\gamma$ ,  $W^\pm$ ,  $Z^0$  and  $H^0$ ), could also be treated in the TMD factorisation framework. One of the crucial aspects yet to be fully understood in this case is whether an imbalance to be measured in the final state can be related to the transverse momentum of the initial partons. For this to be true, final-state gluon emissions should admittedly be suppressed at least to a tractable extent.

For unpolarised colliding protons at the LHC, there are two relevant gluon TMDs: the distribution of unpolarised gluons,  $f_1^g$ , and the distribution of linearly polarised gluons,  $h_1^{\perp g}$ . The latter is of particular interest as this distribution flips the helicity of the gluon entering the partonic cross section. As a result, the linear polarisation of the gluon manifests itself in two ways: a modification of the transverse-momentum dependence of the cross section in a characteristic way, and an azimuthal modulation of the cross section. As a matter of fact, the linear polarisation may serve as a general new tool in particle physics. Examples of the usefulness of the linear gluon polarisation have been discussed in the context of  $H^0$  boson production in [29,30], as well as for  $H^0 + \text{jet}$  production [28].

Like all other TMDs,  $f_1^g$  and  $h_1^{\perp g}$  are affected by the presence of initial and final state interactions, whose effects are encoded in the Wilson lines needed for their gauge-invariant definition. TMD factorisation may therefore fail for some processes, as we already mentioned above. Moreover, TMDs may become process dependent even in those cases where factorisation can be proven. The gluon TMDs appearing in all the proton–proton scattering reactions where only initial state interactions are present, like the ones under study here, correspond to the so called Weiszäcker–Williams distributions in the small  $x$  region. They can be related to gluon TMDs extracted, for example, in heavy quark pair and dijet production in deep-inelastic electron–proton scattering processes [13]. In particular, we expect to probe the same  $f_1^g$  and  $h_1^{\perp g}$  distributions in all such processes, because they are  $T$ -even TMDs. This is a very important property that still needs to be confirmed by experiments. We refer to [21] for further details.

In this paper, we will explore the relevance of final states consisting of a heavy quarkonium, like  $\Upsilon$  or  $J/\psi$ , produced with a dilepton, be it from a  $Z$  boson or from a virtual photon, in the kinematical configuration already mentioned above, such that their transverse momenta are almost back to back. In such a case, we will show how they can help extracting information about the linear polarisation of gluons. Our proposal is motivated by the fact that the detection of a dilepton may experimentally be cleaner or easier compared to the detection of a photon. For instance, the cross section for  $J/\psi$  production in association with a  $Z$  boson has already been studied by the ATLAS Collaboration [31] and compared to theoretical predictions [32–34]. This showed that, in the ATLAS acceptance, a significant contribution from double parton scattering (DPS) is expected, which does not fall in the scope of this work. In what follows, we will assume that constraining both observed particles to be back to back makes the DPS yield small enough and we will not venture into the region of large rapidity separations where it can be dominant. Moreover,  $J/\psi + \gamma$  and  $\Upsilon + \gamma$  have only been investigated [35] – also by ATLAS – in the context of  $H^0$  studies, thus at very large invariant mass where the yields are extremely small and the contributions we are after are a background to the  $H^0$  signal. Studies in the kinematical region considered in [27] or in [36,37] have not yet been done.  $J/\psi(\Upsilon) + W^\pm$  would also be an option since it has also been experimentally studied – still by ATLAS [38] – but it is not dominated by gluon induced reactions [39,40].

The paper is organised as follows: In Section 2 we discuss the gluon fusion process in the TMD factorisation approach for an arbitrary final state and analyse the general structure of the

differential cross section. We then analytically calculate the partonic cross sections for each of the azimuthal structures to leading order (LO) accuracy for the final state  $Q + \ell\bar{\ell}$  where  $Q$  is a spin-triplet vector quarkonium. In Section 3, we give our numerical results for the quarkonium +  $Z$  final state, while numerical results for a quarkonium +  $(\ell\bar{\ell})$  final state are presented in Section 4. We draw our conclusions in Section 5.

## 2. Analytic calculation within the TMD approach

In this section we consider the process  $p(P_a) + p(P_b) \rightarrow Q(P_Q) + \ell(l) + \bar{\ell}(\bar{l}) + X$ , where  $Q$  denotes a heavy quarkonium bound state, in a kinematical regime where the final state momentum  $q^\mu \equiv P_Q^\mu + l^\mu + \bar{l}^\mu \equiv P_Q^\mu + P_B^\mu$  has a small transverse component,  $q_T$ , with respect to the beam axis in the proton centre-of-mass (c.m.) frame. To be precise, the transverse momentum has to be much smaller than the hard scale of the process, e.g. the invariant mass  $Q$  ( $q^2 = Q^2$ ) of the final-state, namely  $q_T \ll Q$ . This is the regime where TMD factorisation can be applied.

Furthermore, we assume that the underlying production mechanism of the heavy quarkonium + lepton pair is due to gluon interactions only. As such, this final state can be considered as a probe for gluon TMDs in proton collisions. In Ref. [27], we have shown that, at the LHC, this is indeed the case for the associated production of a heavy quarkonium and a real photon, instead of a lepton pair.

A second assumption we make here is that the heavy quarkonium is produced directly as a colour-singlet state. For the production of  $\Upsilon - \gamma$  at the LHC, this assumption is valid, but not necessarily for  $J/\psi - \gamma$  [27]. Where needed, such an assumption can be ensured by isolating the quarkonium (as done in [35]).

### 2.1. General structure of the cross section

In a first step we present the fully differential cross section in the TMD approach (cf. Refs. [14, 29,30,11,27,15,9,6]) in a general form as

$$d\sigma_{\text{TMD}} = \frac{(2\pi)^4}{S^2} d\text{PS}_n \frac{1}{(N_c^2 - 1)^2} \sum_{a,b;I} \mathcal{A}_{\mu\nu;I}^{ab}(\bar{k}_a, \bar{k}_b; \{P_i\}) \mathcal{A}_{\rho\sigma;I}^{ab*}(\bar{k}_a, \bar{k}_b; \{P_i\}) \times \int \frac{d^2\mathbf{y}_T}{(2\pi)^2} e^{iq_T \cdot \mathbf{y}_T} \tilde{\Gamma}^{\rho\mu}(x_a, \mathbf{y}_T, \zeta_a, \mu) \tilde{\Gamma}^{\sigma\nu}(x_b, \mathbf{y}_T, \zeta_b, \mu) + O(q_T/Q) \quad (1)$$

$$= \frac{(2\pi)^4}{S^2} d\text{PS}_n \frac{1}{(N_c^2 - 1)^2} \sum_{a,b;I} \mathcal{A}_{\mu\nu;I}^{ab}(\bar{k}_a, \bar{k}_b; \{P_i\}) \mathcal{A}_{\rho\sigma;I}^{ab*}(\bar{k}_a, \bar{k}_b; \{P_i\}) \times \int d^2\mathbf{k}_{aT} \int d^2\mathbf{k}_{bT} \delta^{(2)}(\mathbf{k}_{aT} + \mathbf{k}_{bT} - \mathbf{q}_T) \Gamma^{\rho\mu}(x_a, \mathbf{k}_{aT}, \zeta_a, \mu) \Gamma^{\sigma\nu}(x_b, \mathbf{k}_{bT}, \zeta_b, \mu) + O(q_T/Q), \quad (2)$$

where  $a$  and  $b$  are colour indices,  $N_c = 3$  is the number of colours, and the sum  $\sum_I$  denotes the summation over those indices that can identify the particles in the final state, like their helicity. The differential phase space factor reads  $d\text{PS}_n = \prod_{i=1}^n \frac{d^3p_i}{(2\pi)^3 2E_i}$ , with  $E_i = \sqrt{\mathbf{p}_i^2 + m_i^2}$ . Moreover,  $\mathcal{A}$  denotes the hard scattering amplitude for an arbitrary gluon-induced process  $gg \rightarrow p_1 + \dots + p_n$ , with  $n$  colour-singlet particles of momenta  $P_1, \dots, P_n$  in the final state. It is factorised from the soft part contained in the integral in the second line and can be perturbatively

calculated. The gluon momenta entering this amplitude are approximated as  $\bar{k}_{a/b}^\mu = x_{a/b} P_{a/b}^\mu$ . The longitudinal momentum fractions are set to  $x_a = q \cdot P_b / P_a \cdot P_b$  and  $x_b = q \cdot P_a / P_a \cdot P_b$ , with  $q = P_1 + P_2 + \dots + P_n$ .

The formula in (1) describes an arbitrary gluon-induced process with a colour-singlet final state in the TMD formalism. Here, the  $\bar{\Gamma}$ 's denote the non-perturbative gluonic TMD matrix elements that were properly defined in  $y_T$  coordinate space in Ref. [9], including the renormalisation scale  $\mu$  as well as an additional scale  $\zeta$ . The evolution in  $\zeta$  of the TMD correlator  $\bar{\Gamma}$  is governed by the Collins–Soper evolution equation (cf. Refs. [3,9]). When going from equations (1) to (2), a simple Fourier transform w.r.t.  $y_T$  is performed. Hence,  $\bar{\Gamma}$  and  $\Gamma$  are related via a Fourier transform. In particular,  $\Gamma$  depends on the longitudinal gluon momentum fraction  $x$  and the gluon transverse momentum  $\mathbf{k}_T$ .

The TMD correlator  $\Gamma$  can be parametrised in terms of gluon TMDs (cf. Refs. [1,41]). For an unpolarised nucleon one finds two structures of the following form,

$$\Gamma^{\mu\nu}(x, \mathbf{k}_T) = \frac{1}{2x} \left( -g_T^{\mu\nu} f_1^g(x, \mathbf{k}_T^2) + \frac{k_T^\mu k_T^\nu + \frac{1}{2} \mathbf{k}_T^2 g_T^{\mu\nu}}{M^2} h_1^{\perp g}(x, \mathbf{k}_T^2) \right). \quad (3)$$

The TMD distribution  $f_1^g$  can be interpreted as the distribution of unpolarised gluons in an unpolarised nucleon, while the function  $h_1^{\perp g}$  is the distribution of linearly polarised gluons [1]. In addition, we have introduced the transverse projector  $g_T^{\mu\nu} = g^{\mu\nu} - P^\mu n^\nu - P^\nu n^\mu$ , where  $P$  is the nucleon momentum and  $n$  is an adjoint light-cone vector such that  $n^2 = 0$  and  $P \cdot n = 1$ . Moreover, in (3),  $M$  denotes the nucleon mass. We note that the parametrisation (3) is slightly different from the one in Ref. [9] where the  $M^2$  in (3) is replaced by  $\frac{1}{2} \mathbf{k}_T^2$ . Also, we have an additional factor  $1/x$  in (3).

Getting back to the expression for the cross section in (2), it is useful to consider it in the c.m. frame of both incoming protons, with  $P_{a/b}$  along the positive (negative)  $z$ -direction, e.g.,  $P_{a/b}^\mu = \sqrt{S/2} n_{\pm}^\mu$ , with  $n^\mu = (1, 0, 0, \pm 1)/\sqrt{2}$ . In this frame, we can work with simple polarisation vectors of the gluons (which are approximated to be collinear to the proton momenta in the amplitudes  $\mathcal{A}$  in (2)). One can easily find that these polarisation vectors acquire the following form in terms of the gluon helicities  $\lambda_{a/b} = \pm 1$ ,

$$\varepsilon_{\lambda_a}^\mu(\bar{k}_a) = \left( 0, -\frac{\lambda_a}{\sqrt{2}}, -\frac{i}{\sqrt{2}}, 0 \right); \quad \varepsilon_{\lambda_b}^\mu(\bar{k}_b) = \left( 0, \frac{\lambda_b}{\sqrt{2}}, -\frac{i}{\sqrt{2}}, 0 \right). \quad (4)$$

These polarisation vectors lead to the common polarisation sum in the Feynman gauge,

$$-g_T^{\mu\nu} = \sum_{\lambda_{a/b}} \varepsilon_{\lambda_{a/b}}^\mu(\bar{k}_{a/b}) \varepsilon_{\lambda_{a/b}}^{\nu*}(\bar{k}_{a/b}). \quad (5)$$

In addition, the polarisation vectors are transverse, i.e.,  $\bar{k}_a \cdot \varepsilon_{\lambda_a}(\bar{k}_a) = \bar{k}_b \cdot \varepsilon_{\lambda_b}(\bar{k}_a) = \bar{k}_a \cdot \varepsilon_{\lambda_b}(\bar{k}_b) = \bar{k}_b \cdot \varepsilon_{\lambda_b}(\bar{k}_b) = 0$ . Of course, the polarisation vectors (4) are only determined up to a phase, therefore other realisations are possible as well.

Since the contraction of Minkowski indices  $\mu, \nu, \rho, \sigma$  in (2) is to be understood as a contraction in the *transverse* space, we can insert the polarisation sums (5) and rewrite (2) in terms of the helicity amplitudes,

$$d\sigma_{\text{TMD}} = \frac{(2\pi)^4}{S^2} d\text{PS}_n \sum_{\lambda_a, \bar{\lambda}_a, \lambda_b, \bar{\lambda}_b = \pm 1} \frac{1}{(N_c^2 - 1)^2} \sum_{a,b;I} \mathcal{A}_{\lambda_a, \lambda_b; I}^{ab}(\bar{k}_a, \bar{k}_b; \{P_i\}) \times$$

$$\mathcal{A}_{\bar{\lambda}_a, \bar{\lambda}_b; I}^{ab*}(\bar{k}_a, \bar{k}_b; \{P_i\}) \int d^2\mathbf{k}_{aT} \int d^2\mathbf{k}_{bT} \delta^{(2)}(\mathbf{k}_{aT} + \mathbf{k}_{bT} - \mathbf{q}_T) \Gamma_{\bar{\lambda}_a, \lambda_a}(x_a, \mathbf{k}_{aT}, \zeta_a, \mu) \times \Gamma_{\bar{\lambda}_b, \lambda_b}(x_b, \mathbf{k}_{bT}, \zeta_b, \mu) + O(q_T/Q). \quad (6)$$

Here, we introduced the notation  $\mathcal{A}_{\lambda_a, \lambda_b} \equiv \varepsilon_{\lambda_a}^\mu(\bar{k}_a) \varepsilon_{\lambda_b}^\nu(\bar{k}_b) \mathcal{A}_{\mu\nu}$  for the helicity amplitudes, and the helicity gluon correlator  $\Gamma_{\bar{\lambda}, \lambda} \equiv (\varepsilon_{\bar{\lambda}}^\mu(\bar{k}) \varepsilon_{\lambda}^{\nu*}(\bar{k}) \Gamma_{\mu\nu})$ . For an unpolarised nucleon the parameterisation in terms of the gluon helicities then takes the following form,

$$\Gamma_{\bar{\lambda}_a, \lambda_a}(x_a, \mathbf{k}_{aT}) = \frac{1}{2x_a} \left( \delta_{\lambda_a, \bar{\lambda}_a} f_1^g(x_a, \mathbf{k}_{aT}^2) + \frac{k_{ax}^2 - k_{ay}^2 - 2i\lambda_a k_{ax} k_{ay}}{2M^2} \delta_{\lambda_a, -\bar{\lambda}_a} h_1^{\perp g}(x_a, \mathbf{k}_{aT}^2) \right), \quad (7)$$

$$\Gamma_{\bar{\lambda}_b, \lambda_b}(x_b, \mathbf{k}_{bT}) = \frac{1}{2x_b} \left( \delta_{\lambda_b, \bar{\lambda}_b} f_1^g(x_b, \mathbf{k}_{bT}^2) + \frac{k_{bx}^2 - k_{by}^2 + 2i\lambda_b k_{bx} k_{by}}{2M^2} \delta_{\lambda_b, -\bar{\lambda}_b} h_1^{\perp g}(x_b, \mathbf{k}_{bT}^2) \right), \quad (8)$$

with  $\mathbf{k}_{aT} = (k_{ax}, k_{ay})$  and  $\mathbf{k}_{bT} = (k_{bx}, k_{by})$ . It is evident from (7), (8) that the gluon TMD  $f_1^g$  conserves the gluon helicity at the non-perturbative level, while the distribution of linearly polarised gluons,  $h_1^{\perp g}$ , flips it. We can insert the parameterisations (7), (8) into (6) and write the differential cross section in the general form

$$d\sigma_{\text{TMD}} = \frac{(2\pi)^4}{4x_a x_b S^2} d\text{PS}_n \left\{ \hat{F}_1(\bar{k}_a, \bar{k}_b; \{P_i\}) C[f_1^g f_1^g] + \hat{F}_2(\bar{k}_a, \bar{k}_b; \{P_i\}) C[w_2 h_1^{\perp g} h_1^{\perp g}] + \hat{F}_3a(\bar{k}_a, \bar{k}_b; \{P_i\}) C[w_{3a} h_1^{\perp g} f_1^g] + \hat{F}_3b(\bar{k}_a, \bar{k}_b; \{P_i\}) C[w_{3b} f_1^g h_1^{\perp g}] + \hat{F}_4(\bar{k}_a, \bar{k}_b; \{P_i\}) C[w_4 h_1^{\perp g} h_1^{\perp g}] \right\} + O(q_T/Q), \quad (9)$$

where the different transverse momentum convolutions of gluon TMDs are abbreviated as

$$C[w f g] \equiv \int d^2\mathbf{k}_{aT} \int d^2\mathbf{k}_{bT} \delta^{(2)}(\mathbf{k}_{aT} + \mathbf{k}_{bT} - \mathbf{q}_T) w(\mathbf{k}_{aT}, \mathbf{k}_{bT}, \mathbf{q}_T) \times f(x_a, \mathbf{k}_{aT}^2) g(x_b, \mathbf{k}_{bT}^2). \quad (10)$$

Since the distribution of linearly polarised gluons carries gluon transverse-momentum-dependent prefactors in the parameterisations (7), (8), these prefactors emerge again in the convolutions in (9) in the weighting factors  $w$ . To be specific we have

$$w_2 = \frac{2(\mathbf{k}_{aT} \cdot \mathbf{k}_{bT})^2 - \mathbf{k}_{aT}^2 \mathbf{k}_{bT}^2}{4M^4},$$

$$w_4 = 2 \left[ \frac{\mathbf{k}_{aT} \cdot \mathbf{k}_{bT}}{2M^2} - \frac{(\mathbf{k}_{aT} \cdot \mathbf{q}_T)(\mathbf{k}_{bT} \cdot \mathbf{q}_T)}{M^2 \mathbf{q}_T^2} \right]^2 - \frac{\mathbf{k}_{aT}^2 \mathbf{k}_{bT}^2}{4M^4},$$

$$w_{3a} = \frac{\mathbf{k}_{aT}^2 \mathbf{q}_T^2 - 2(\mathbf{q}_T \cdot \mathbf{k}_{aT})^2}{2M^2 \mathbf{q}_T^2}, \quad w_{3b} = \frac{\mathbf{k}_{bT}^2 \mathbf{q}_T^2 - 2(\mathbf{q}_T \cdot \mathbf{k}_{bT})^2}{2M^2 \mathbf{q}_T^2}. \quad (11)$$

We find five different structures in the cross section in (9): the first one is given by a convolution of two unpolarised gluon TMDs, while the second and fifth are given by the convolutions of two distributions of linearly polarised gluons. In the latter case the helicities of each gluon are flipped. We separated both these structures because the second typically provides azimuthally

isotropic contributions, while the fifth leads to azimuthal modulations (around the beam axis) of the differential cross section. The third and fourth structures are mixed convolutions of an unpolarised and a linearly polarised gluon TMD. Here, only one of the gluon helicities is flipped.

The factors  $\hat{F}_i$  in (9) can be calculated perturbatively since they are defined in terms of the partonic amplitudes  $\mathcal{A}$  in the following way,

$$\begin{aligned}\hat{F}_1(\bar{k}_a, \bar{k}_b; \{P_i\}) &= \sum_{\lambda_a, \lambda_b, =\pm 1} \frac{1}{(N_c^2 - 1)^2} \sum_I \mathcal{A}_{\lambda_a, \lambda_b; I}^{ab}(\bar{k}_a, \bar{k}_b; \{P_i\}) \mathcal{A}_{\lambda_a, \lambda_b; I}^{ab*}(\bar{k}_a, \bar{k}_b; \{P_i\}), \\ \hat{F}_2(\bar{k}_a, \bar{k}_b; \{P_i\}) &= \sum_{\lambda=\pm 1} \frac{1}{(N_c^2 - 1)^2} \sum_I \mathcal{A}_{\lambda, \lambda; I}^{ab}(\bar{k}_a, \bar{k}_b; \{P_i\}) \mathcal{A}_{-\lambda, -\lambda; I}^{ab*}(\bar{k}_a, \bar{k}_b; \{P_i\}), \\ \hat{F}_{3a}(\bar{k}_a, \bar{k}_b; \{P_i\}) &= \sum_{\lambda_a, \lambda_b, =\pm 1} \frac{1}{(N_c^2 - 1)^2} \sum_I \mathcal{A}_{\lambda_a, \lambda_b; I}^{ab}(\bar{k}_a, \bar{k}_b; \{P_i\}) \mathcal{A}_{-\lambda_a, \lambda_b; I}^{ab*}(\bar{k}_a, \bar{k}_b; \{P_i\}), \\ \hat{F}_{3b}(\bar{k}_a, \bar{k}_b; \{P_i\}) &= \sum_{\lambda_a, \lambda_b, =\pm 1} \frac{1}{(N_c^2 - 1)^2} \sum_I \mathcal{A}_{\lambda_a, \lambda_b; I}^{ab}(\bar{k}_a, \bar{k}_b; \{P_i\}) \mathcal{A}_{\lambda_a, -\lambda_b; I}^{ab*}(\bar{k}_a, \bar{k}_b; \{P_i\}), \\ \hat{F}_4(\bar{k}_a, \bar{k}_b; \{P_i\}) &= \sum_{\lambda=\pm 1} \frac{1}{(N_c^2 - 1)^2} \sum_I \mathcal{A}_{\lambda, -\lambda; I}^{ab}(\bar{k}_a, \bar{k}_b; \{P_i\}) \mathcal{A}_{-\lambda, \lambda; I}^{ab*}(\bar{k}_a, \bar{k}_b; \{P_i\}).\end{aligned}\quad (12)$$

The results in (9)–(12) are the main ones of this subsection, and are valid for an arbitrary process induced by the interaction of two gluons in the initial state, where a colour-singlet final state is produced. In the following, we will analyse a specific hadronic reaction in which a heavy quarkonium state and a lepton pair are produced back to back in transverse space.

## 2.2. The subprocess $gg \rightarrow Q\ell\bar{\ell}$

### 2.2.1. The helicity structure

We will now compute the amplitude  $\mathcal{A}$  for the process  $gg \rightarrow Q\ell\bar{\ell}$  and use these results to determine the explicit expressions of the  $\hat{F}_i$  in (9). The first observation we make is that the lepton pair is produced either through the decay of a virtual photon or a  $Z$  boson. Hence, we can decompose the amplitude further and write

$$\mathcal{A}_{\lambda_a, \lambda_b}^{gg \rightarrow Q\ell\bar{\ell}} = \sum_{j=\gamma^*, Z} i C_j \mathcal{A}_{\lambda_a, \lambda_b}^{gg \rightarrow Qj; \mu} \frac{g_{\mu\nu} - P_{B\mu} P_{B\nu} / M_B^2}{M_B^2 - \Delta_j} \bar{u}(l, \sigma) \gamma^\nu (a_j + b_j \gamma_5) v(\bar{l}, \bar{\sigma}).\quad (13)$$

Here,  $M_B^2 = P_B^2$  denotes the virtuality of the electroweak gauge boson. In addition, we introduced the constants  $C_{\gamma^*} = -4\pi\alpha_{\text{em}}$ ,  $C_Z = m_Z^2 G_F / 2 / \sqrt{2}$ , where  $\alpha_{\text{em}}$  is the electromagnetic fine structure constant,  $G_F$  Fermi's constant, and  $m_Z$  the mass of the  $Z$  boson. The poles of the electroweak propagators are  $\Delta_{\gamma^*} = 0$  and  $\Delta_Z = m_Z^2 - i\Gamma_Z m_Z$ , where  $\Gamma_Z$  is the total width of the  $Z$  boson. The electroweak coupling to the leptons involves the constants  $a_{\gamma^*} = 1$ ,  $b_{\gamma^*} = 0$  for a virtual photon, and  $a_Z = 3 - 4m_Z^2/m_W^2$ ,  $b_Z = 1$  for a  $Z$  boson, where  $m_W$  is the mass of the  $W$  boson.

With the decomposition (13) at hand we can calculate the amplitude squared,

$$\begin{aligned}
 \mathcal{F}_{\lambda_a \lambda_b; \bar{\lambda}_a \bar{\lambda}_b} &\equiv \frac{(2\pi)^4}{4x_a x_b S^2} \frac{d\text{PS}_3}{(N_c^2 - 1)^2} \sum_I \mathcal{A}_{\lambda_a, \lambda_b; I}^{gg \rightarrow Q \ell \bar{\ell}} \mathcal{A}_{\bar{\lambda}_a, \bar{\lambda}_b; I}^{* gg \rightarrow Q \ell \bar{\ell}} \\
 &= \frac{1}{4(2\pi)^5 x_a x_b S^2 (N_c^2 - 1)^2} \frac{d^3 P_Q}{2E_Q} \times \\
 &\quad \left( \sum_{j, \bar{j} = \gamma^*, Z} C_j C_{\bar{j}} \sum_I \mathcal{A}_{\lambda_a, \lambda_b; I}^{gg \rightarrow Q, j; \mu} \mathcal{A}_{\bar{\lambda}_a, \bar{\lambda}_b; I}^{* gg \rightarrow Q, \bar{j}; \rho} \frac{g_{\mu\nu} - P_{B\mu} P_{B\nu} / M_B^2}{(M_B^2 - \Delta_j)} \times \right. \\
 &\quad \left. \frac{g_{\rho\sigma} - P_{B\rho} P_{B\sigma} / M_B^2}{(M_B^2 - \Delta_{\bar{j}})^*} \left[ L_{j\bar{j}}^{\nu\sigma}(l, \bar{l}) d^4 l \delta(l^2) \theta(l^0) d^4 \bar{l} \delta(\bar{l}^2) \theta(\bar{l}^0) \right] \right). \tag{14}
 \end{aligned}$$

We note that any explicit dependence on the single lepton momenta is hidden in the last line, where we have introduced the Lorentz-invariant leptonic tensor

$$L_{j\bar{j}}^{\nu\sigma} = 4(a_j a_{\bar{j}} + b_j b_{\bar{j}}) \left( l^\nu \bar{l}^\sigma + l^\sigma \bar{l}^\nu - \frac{1}{2} M_B^2 g^{\nu\sigma} \right) + 4(a_j b_{\bar{j}} + b_j a_{\bar{j}}) \epsilon^{\nu\sigma\eta\kappa} l_\eta \bar{l}_\kappa. \tag{15}$$

We now integrate over the momentum  $\bar{l}$  of the antilepton, keeping in mind that  $d^4 l d^4 \bar{l} \delta(l^2) \delta(\bar{l}^2) = d^4 P_B d^4 \bar{l} \delta(\bar{l}^2) \delta((P_B - \bar{l})^2)$ . Since the last line of (14) is Lorentz-invariant, this is conveniently done in the centre-of-mass frame of the lepton pair where the pair momentum takes the simple form  $P_B^\mu = (M_B, 0, 0, 0)$ . The delta functions are easily integrated out, and we find  $d^4 l d^4 \bar{l} \delta(l^2) \delta(\bar{l}^2) \rightarrow \frac{1}{8} d^4 P_B d\Omega$ , with  $\Omega$  the solid angle which determines the direction of the antilepton. Using an explicit form of the antilepton momentum  $\bar{l}^\mu = \frac{M_B}{2}(1, \vec{e})$  with  $\vec{e} = (\sin\theta \cos\phi, \sin\theta \sin\phi, \cos\theta)$  in this specific dilepton c.m.-frame we can perform the solid angle integration and obtain

$$\begin{aligned}
 \int d\Omega L_{j\bar{j}}^{\nu\sigma} &= \int d\Omega 4 \left[ (a_j a_{\bar{j}} + b_j b_{\bar{j}}) \left( -2\bar{l}^\nu \bar{l}^\sigma + P_B^\nu \bar{l}^\sigma + P_B^\sigma \bar{l}^\nu - \frac{1}{2} M_B^2 g^{\nu\sigma} \right) \right. \\
 &\quad \left. + (a_j b_{\bar{j}} + b_j a_{\bar{j}}) \epsilon^{\nu\sigma\eta\kappa} P_{B\eta} \bar{l}_\kappa \right] \\
 &= \frac{16}{3} \pi (a_j a_{\bar{j}} + b_j b_{\bar{j}}) \left( P_B^\nu P_B^\sigma - M_B^2 g^{\nu\sigma} \right). \tag{16}
 \end{aligned}$$

We insert this result into the quantity  $\mathcal{F}$  in (14) and perform the contraction with the numerators of the weak boson-propagators. This leads to a factor  $-M_B^2 (g_{\mu\rho} - P_{B\mu} P_{B\rho} / M_B^2)$  coming from  $M_B^2 \sum_{\lambda_B=0, \pm 1} \epsilon_{\mu, \lambda_B}^* (P_B) \epsilon_{\rho, \lambda_B} (P_B)$  in the numerator, which we have identified as the sum over the helicities of the polarisation vectors of the virtual electroweak boson. Note that, since the virtual electroweak boson is massive (formally carrying a mass  $P_B^2 = M_B^2$ ), three polarisations are necessary. Utilising the polarisation sum in this way allows us to work with helicity amplitudes when calculating the process  $gg \rightarrow Q\gamma^*/Z$ .

Finally, we also need to modify the remaining phase space  $d^4 P_Q d^4 P_B \delta(P_Q^2 - M_Q^2) \theta(P_Q^0)$  where  $M_Q$  is the mass of the heavy quarkonium state. We do so by considering the relative momenta  $q^\mu = P_Q^\mu + P_B^\mu$  and  $\Delta q^\mu = P_Q^\mu - P_B^\mu$  and note that  $d^4 P_B d^4 P_Q = \frac{1}{16} d^4 q d^4 \Delta q$ . It is most convenient to analyse these factors in a c.m.-frame of the heavy quarkonium and the virtual electroweak gauge boson, such as the Collins–Soper (CS) frame. In this frame the gluon momenta are along the  $z$ -axis whereas the heavy quarkonium and electroweak gauge boson momenta have an explicit representation in this frame,  $P_Q^\mu = \left( \sqrt{\Lambda^2 + M_Q^2}, \Lambda \vec{e} \right)$  and

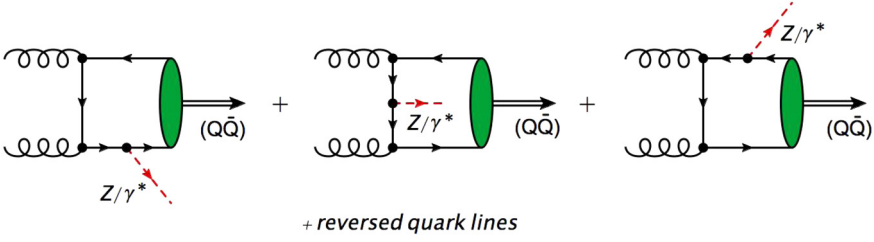


Fig. 1. Leading order diagrams for the subprocess  $gg \rightarrow QZ/\gamma^*$ . Diagrams where the direction of the quark lines are reversed also contribute. (For interpretation of the references to colour in this figure, the reader is referred to the web version of this article.)

$P_B^\mu = \left( \sqrt{\Lambda^2 + M_B^2}, -\Lambda \vec{e} \right)$ , with  $\vec{e} = (\sin\theta \cos\phi, \sin\theta \sin\phi, \cos\theta)$  as before, where  $\theta$  and  $\phi$  are the Collins–Soper angles. From considering  $q^2 = (P_Q + P_B)^2 \equiv Q^2 > 0$  we find that  $\Lambda = \sqrt{\lambda(Q^2, M_Q^2, M_B^2)}/(2Q)$ , with  $\lambda(x, y, z) = x^2 + y^2 + z^2 - 2xy - 2xz - 2yz$ . Hence, the relative momenta take the explicit form  $q^\mu = (Q, 0, 0, 0)$  and  $\Delta q^\mu = ((M_Q^2 - M_B^2)/Q, 2\Lambda \vec{e})$  in the CS frame, and we conclude that  $d^4P_Q d^4P_B \delta(P_Q^2 - M_Q^2) \theta(P_Q^0) \rightarrow \Lambda/(4Q) d^4q dM_B^2 d\Omega$ . Collecting all the results above, we rewrite (14) as

$$\mathcal{F}_{\lambda_a \lambda_b; \bar{\lambda}_a \bar{\lambda}_b} = \frac{\Lambda M_B^2}{48 (2\pi)^4 x_a x_b S^2 Q (N_c^2 - 1)^2} d^4q dM_B^2 d\Omega \times \left( \sum_{j, \bar{j}=\gamma^*, Z} \frac{C_j C_{\bar{j}} (a_j a_{\bar{j}} + b_j b_{\bar{j}})}{(M_B^2 - \Delta_j) (M_B^2 - \Delta_{\bar{j}})^*} \sum_{\lambda_B=0, \pm 1; I} \mathcal{A}_{\lambda_a, \lambda_b; \lambda_B; I}^{gg \rightarrow Q, j} \mathcal{A}_{\bar{\lambda}_a, \bar{\lambda}_b; \lambda_B; I}^{* gg \rightarrow Q, \bar{j}} \right). \quad (17)$$

### 2.2.2. The amplitude $\mathcal{A}^{gg \rightarrow Q(Z/\gamma^*)}$

As a final step, we need to calculate the amplitude  $\mathcal{A}^{gg \rightarrow Q(Z/\gamma^*)}$ . We will do so to leading order accuracy in perturbative QCD and assume a colour-singlet heavy quarkonium state. The leading order diagrams are shown in Fig. 1. In the following we restrict ourselves to heavy quarkonium states without orbital angular momentum quantum numbers, in particular to a  $J/\psi$  or  $\Upsilon$  state. In the colour-singlet model one typically neglects relative momenta of the heavy quark–antiquark pair in the hard part such that the wave function of the heavy quarkonium state shrinks to the origin, and the vertex of the transition of both heavy quarks forming a  $J/\psi$  or  $\Upsilon$  – the green blobs in Fig. 1 – reduces to a vertex  $1/\sqrt{4\pi N_c M_Q} R_0(0) (\not{P}_Q - M_Q) \not{\epsilon}_{\lambda_Q}(P_Q)$ , where  $R_0(0)$  is the radial wave function of the heavy quarkonium state at the origin in the quarkonium rest frame, and  $\epsilon_{\lambda_Q}(P_Q)$  the polarisation vector of the  $J/\psi$  or  $\Upsilon$  (cf. Ref. [15]). Note that we have again three polarisations  $\lambda_Q = 0, \pm 1$  for a massive spin-1 particle. We also note that the coupling of the electroweak gauge boson depends on the flavor of the quark, i.e., we have a quark–gauge boson vertex of the form  $\gamma^\mu (a_q + b_q \gamma_5)$ , with  $a_c = -5/3 + (8/3)m_W^2/m_Z^2$ ,  $b_c = -1$  for a charm quark coupling to a Z-boson,  $a_b = 7/3 - (4/3)m_W^2/m_Z^2$ ,  $b_b = +1$  for a bottom quark coupling to a Z-boson, and  $a_c = a_b = 1$ ,  $b_c = b_b = 0$  for a quark coupling to a photon.

The leading order diagrams can then be calculated in a straightforward way, and we will not elaborate on the details of the calculation. Once we have obtained the analytic expressions for

the helicity amplitudes  $\mathcal{A}^{gg \rightarrow J/\psi[\Upsilon](Z/\gamma^*)}$  we insert them into (17). It is then only a minor step to extract the  $\hat{F}_i$ -prefactors in (12).

2.2.3. The azimuthal dependence of the differential cross section

To go further, we decompose, in the CS frame, the differential cross section in terms of factors  $\hat{F}_i$ :

$$\begin{aligned} & \frac{d\sigma_{\text{TMD, LO}}^{pp \rightarrow J/\psi[\Upsilon]\ell\bar{\ell}X}}{d^4q dM_B^2 d\Omega} \\ &= \hat{F}_1(Q, \alpha, \beta, \theta) C[f_1^g f_1^g] + \hat{F}_2(Q, \alpha, \beta, \theta) C[w_2 h_1^{\perp g} h_1^{\perp g}] \\ &+ \left\{ \hat{F}_{3a}(Q, \alpha, \beta, \theta) C[w_{3a} h_1^{\perp g} f_1^g] + \hat{F}_{3b}(Q, \alpha, \beta, \theta) C[w_{3b} f_1^g h_1^{\perp g}] \right\} \cos 2\phi \\ &+ \hat{F}_4(Q, \alpha, \beta, \theta) C[w_4 h_1^{\perp g} h_1^{\perp g}] \cos 4\phi, \end{aligned} \tag{18}$$

where the  $\hat{F}_i$  are functions of the  $\theta$  CS-angle, the parameters  $\alpha \equiv M_Q/Q$  and  $\beta \equiv M_B/Q$ . The prefactors  $\hat{F}_i$  have the form

$$\hat{F}_i = \frac{4\alpha_s^2 |R_0(0)|^2 \Lambda M_B^2}{3\pi^3 x_a x_b S^2 Q^3 M_Q N_c (N_c^2 - 1)^2} \sum_{j, \bar{j}=\gamma^*, Z} \frac{\tilde{C}_j \tilde{C}_{\bar{j}} (a_j a_{\bar{j}} + b_j b_{\bar{j}})}{(M_B^2 - \Delta_j)(M_B^2 - \Delta_{\bar{j}})^*} \frac{\hat{f}_i(\alpha, \beta, \theta)}{\hat{D}(\alpha, \beta, \theta)}, \tag{19}$$

where  $\tilde{C}_{\gamma^*} = -4\pi\alpha_{\text{em}}e_q$  and  $\tilde{C}_Z = m_Z^2 G_F a_q / (2\sqrt{2})$ , and  $\Lambda = \frac{Q}{2} \sqrt{\lambda(1, \alpha^2, \beta^2)}$ . The functions  $\hat{f}_i, \hat{D}$  acquire the following form in terms of the auxiliary variables  $A \equiv 1 + \alpha^2 - \beta^2$  and  $B \equiv \sqrt{A^2 - 4\alpha^2} = \sqrt{\lambda(1, \alpha^2, \beta^2)} \geq 0$ ,

$$\hat{D}(\alpha, \beta, \theta) = (2 - A)^2 (A^2 - B^2 \cos^2 \theta)^2, \tag{20}$$

as well as

$$\begin{aligned} \hat{f}_1(\alpha, \beta, \theta) &= a_{1,0} + a_{1,2} \sin^2 \theta + a_{1,4} \sin^4 \theta, \\ \hat{f}_2(\alpha, \beta, \theta) &= a_{2,0}, \\ \hat{f}_{3a}(\alpha, \beta, \theta) &= a_{3,0} \sin^2 \theta = \hat{f}_{3b}(\alpha, \beta, \theta), \\ \hat{f}_4(\alpha, \beta, \theta) &= a_{4,0} \sin^4 \theta, \end{aligned} \tag{21}$$

with

$$\begin{aligned} a_{1,0} &= 16\alpha^2 \left[ 2(1 - \alpha^2)(1 - \alpha^2 + \beta^2) + \alpha^2 \beta^2 \right], \\ a_{1,2} &= 8 \left[ (\alpha - \beta)^2 - 1 \right] \left[ (\alpha + \beta)^2 - 1 \right] \left[ (\alpha^2 - \beta^2)^2 - 2\alpha^2 \right], \\ a_{1,4} &= \left( 2\alpha^2 + \beta^2 \right) \left[ 1 - 2(\alpha^2 + \beta^2) + (\alpha^2 - \beta^2)^2 \right]^2, \\ a_{2,0} &= 48\alpha^4 \beta^2, \\ a_{3,0} &= 8\alpha^2 (\alpha^2 + 2\beta^2) \left[ 1 - 2(\alpha^2 + \beta^2) + (\alpha^2 - \beta^2)^2 \right], \\ a_{4,0} &= a_{1,4}. \end{aligned} \tag{22}$$

Note that in the limit of real photon production, that is,  $M_B \rightarrow 0$  or  $\beta \rightarrow 0$ , we recover the results of the  $\hat{F}_i$  that were found in Ref. [27]. We find that the partonic prefactor  $\hat{f}_2$  vanishes in the real photon limit – a unique feature of this particular final state.

At this point, we would like to remind the reader that, in a NLO calculation of the hard coefficients  $\hat{F}_i$  in Eq. (18), logarithms of the ratios  $\alpha$  and  $\beta$  may appear (see, e.g., Refs. [42,43] for a related study of the Higgs + jet final state). These logarithms may be large if the ratios  $\alpha$  or  $\beta$  are small and may slow down the convergence of the perturbative series. While TMD factorisation mainly concerns a resummation procedure of logarithms of  $q_T/Q$ , it in general does not include resummations of other logarithms. Since we are mainly interested in  $q_T$ -distributions at fixed invariant mass  $Q$ , we will consider logarithms of  $\alpha$  and  $\beta$  as fixed, unlike logarithms of  $q_T/Q$ . A correct treatment of logarithms of  $\alpha$  and  $\beta$  is however beyond the scope of this article and may be the subject of future investigations.

Eqs. (18)–(22) constitute the main analytical results of this work. It is however instructive to analyse the cross section that is integrated over the CS angles including a possible azimuthal weighting factor. These weighting factors may enable us to disentangle the various azimuthal contributions in (18). For example, analogously to Ref. [27], we can deduce the following weighted cross sections from (18),

$$\begin{aligned}
 N^{(0)} &\equiv \int d\Omega \frac{d\sigma_{\text{TMD, LO}}^{pp \rightarrow J/\psi[\Upsilon]\ell\bar{\ell}X}}{d^4q dM_B^2 d\Omega} = \frac{d\sigma_{\text{TMD, LO}}^{pp \rightarrow J/\psi[\Upsilon]\ell\bar{\ell}X}}{d^4q dM_B^2} \\
 &= \hat{F}_1(Q, \alpha, \beta) C[f_1^g f_1^g] + \hat{F}_2(Q, \alpha, \beta) C[w_2 h_1^{\perp g} h_1^{\perp g}], \\
 N^{(2)} &\equiv \int d\Omega \cos 2\phi \frac{d\sigma_{\text{TMD, LO}}^{pp \rightarrow J/\psi[\Upsilon]\ell\bar{\ell}X}}{d^4q dM_B^2 d\Omega} \\
 &= \hat{F}_3(Q, \alpha, \beta) \left( C[w_{3a} h_1^{\perp g} f_1^g] + C[w_{3b} f_1^g h_1^{\perp g}] \right), \\
 N^{(4)} &\equiv \int d\Omega \cos 4\phi \frac{d\sigma_{\text{TMD, LO}}^{pp \rightarrow J/\psi[\Upsilon]\ell\bar{\ell}X}}{d^4q dM_B^2 d\Omega} = \hat{F}_4(Q, \alpha, \beta) C[w_4 h_1^{\perp g} h_1^{\perp g}]. \tag{23}
 \end{aligned}$$

Note that we use the same symbols  $\hat{F}_i$  for the integrated or weighted partonic prefactors, i.e.,  $\hat{F}_{1,2}(Q, \alpha, \beta) = 2\pi \int d\theta \hat{F}_{1,2}(Q, \alpha, \beta, \theta)$  and  $\hat{F}_{3,4}(Q, \alpha, \beta) = \pi \int d\theta \hat{F}_{3a/b,4}(Q, \alpha, \beta, \theta)$ . The  $\theta$ -integration can be performed analytically, and we find the following integrated partonic prefactors utilising Eqs. (19)–(22),

$$\begin{aligned}
 \hat{F}_1(Q, \alpha, \beta) &= \frac{\hat{F}}{(2-A)^2 A^2 B^4} \left[ \frac{B^4 a_{1,0}}{4\alpha^2} - B^2 a_{1,2} + (3A^2 - B^2) a_{1,4} \right. \\
 &\quad \left. + \left( B^4 a_{1,0} + B^2(A^2 + B^2) a_{1,2} - 4\alpha^2 (3A^2 + B^2) a_{1,4} \right) \frac{\ln\left(\frac{A+B}{A-B}\right)}{2AB} \right], \tag{24}
 \end{aligned}$$

$$\hat{F}_2(Q, \alpha, \beta) = \frac{\hat{F} a_{2,0}}{(2-A)^2 A^2} \left[ \frac{1}{4\alpha^2} + \frac{\ln\left(\frac{A+B}{A-B}\right)}{2AB} \right], \tag{25}$$

$$\hat{F}_3(Q, \alpha, \beta) = -\frac{\hat{F} a_{3,0}}{2(2-A)^2 A^2 B^2} \left[ 1 - (A^2 + B^2) \frac{\ln\left(\frac{A+B}{A-B}\right)}{2AB} \right], \quad (26)$$

$$\hat{F}_4(Q, \alpha, \beta) = \frac{\hat{F} a_{4,0}}{2(2-A)^2 A^2 B^4} \left[ 3A^2 - B^2 - 4\alpha^2 (3A^2 + B^2) \frac{\ln\left(\frac{A+B}{A-B}\right)}{2AB} \right]. \quad (27)$$

where we have used the definition

$$\hat{F} \equiv \frac{8\alpha_s^2 |R_0(0)|^2 \Lambda M_B^2}{3\pi^2 x_a x_b S^2 Q^3 M_Q N_c (N_c^2 - 1)^2} \sum_{j, \bar{j}=\gamma^*, Z} \frac{\tilde{C}_j \tilde{C}_{\bar{j}} (a_j a_{\bar{j}} + b_j b_{\bar{j}})}{(M_B^2 - \Delta_j) (M_B^2 - \Delta_{\bar{j}})^*}. \quad (28)$$

The advantage of the quantities  $N^{(i)}$  is that they are – in principle – Lorentz-invariant after having integrated out the CS-angles. Hence, they can be evaluated directly in the hadron c.m.-frame, i.e., the lab frame at the LHC.

However, there are three drawbacks in integrating in  $\theta$ : first, at NLO, one may face large logarithms of  $\sin(\theta)$  for configurations with large rapidity separations for large pair invariant masses [42,43]. Another reason to avoid this region is that it may be populated by Double-Parton-Scattering (DPS) contributions for which the quarkonium and the dilepton production is uncorrelated and can result in large-rapidity separation configurations along the  $z$  axis [44–46]. Finally, detectors like those of ATLAS and CMS, despite their wide rapidity coverage, would not allow for the detection of far forward or backward quarkonium and dileptons. That being said, for the purpose of our exploratory study, such an integration on  $\theta$ , which provides cross-section upper limits, remains valuable.

Below we use these formulae to estimate the size of the effects from linearly polarised gluons that one can expect at the LHC by measuring the associated heavy-quarkonium +  $Z$ -final state.

### 3. Numerical predictions for an associated quarkonium + $Z$ -final state

We can numerically compare the relative size of both contributions from unpolarised and linearly polarised gluons to the angular-integrated cross section  $N^{(0)}$  in (23) by considering the LO ratios  $\hat{F}_{2,3,4}(Q, \alpha, \beta)/\hat{F}_1(Q, \alpha, \beta)$  from Eqs. (24)–(27). In this section, we focus on the production of a (quasi)-real  $Z$ -boson, i.e., dileptons with an invariant mass around the  $Z$ -pole mass  $M_B \simeq m_Z$ . To this end, we consider a  $M_B$ -bin around  $m_Z$  with a bin size of, say, 2 GeV. Hence, we *define* cross sections for real  $Z$ -boson production in the following way,

$$\frac{d\sigma^{pp \rightarrow J/\psi[\Upsilon]ZX}}{d^4q} \equiv \int_{m_Z-1 \text{ GeV}}^{m_Z+1 \text{ GeV}} dM_B \frac{d\sigma^{pp \rightarrow J/\psi[\Upsilon]\ell\bar{\ell}X}}{d^4q dM_B^2}. \quad (29)$$

The structures of the corresponding quantities  $N^{(i)}$  in (23) remain valid for real  $Z$ -boson production, but with integrated partonic prefactors

$$\hat{F}_i^Z(Q, \alpha) = 2Q^2 \int_{\frac{m_Z-1 \text{ GeV}}{Q}}^{\frac{m_Z+1 \text{ GeV}}{Q}} d\beta \beta \hat{F}_i(Q, \alpha, \beta). \quad (30)$$

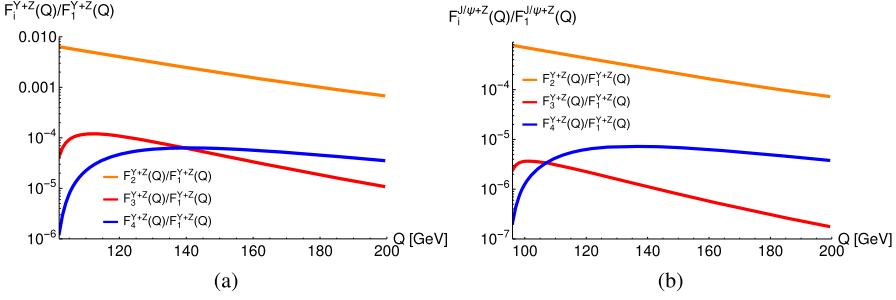


Fig. 2. The ratios  $\hat{F}_{2,3,4}^Z(Q)/\hat{F}_1^Z(Q)$  from (30) plotted vs. the invariant final-state mass  $Q \geq M_Q + m_Z$  for a  $\Upsilon$  (a) and a  $J/\psi$  (b).

The LO ratios  $\hat{F}_{2,3,4}^Z(Q, \alpha, \beta)/\hat{F}_1^Z(Q, \alpha, \beta)$  for real Z-boson productions are shown in Fig. 2. In the left plot we present our result for an associated  $\Upsilon$  state with mass  $m_\Upsilon = 9.46$  GeV. In the right plot, we have shown it for a  $J/\psi$  state with mass  $m_{J/\psi} = 3.1$  GeV. First of all, we observe that the ratios are rather small in general: the ratio  $F_2/F_1$  is about half of a percent at most for  $\Upsilon$ -production and even smaller ( $\leq 10^{-3}$ ) for  $J/\psi$  production. One can expect that the convolution  $C[w_2 h_1^{\perp g} h_1^{\perp g}]$  in (23) from linearly polarised gluons does not exceed in size the convolution  $C[f_1^g f_1^g]$  [29,8]. For example, the models of Ref. [8] indicate that the (scale-dependent) ratio  $R = C[w_2 h_1^{\perp g} h_1^{\perp g}]/C[f_1^g f_1^g]$  is *at most* about  $2/3$  for a small scale  $Q \sim 3$  GeV, but typically (much) smaller for larger scales. Hence, it is not unreasonable to neglect the contribution from linearly polarised gluons for the quantity  $N^{(0)}$  in (23) and approximate to good accuracy,

$$N^{(0)} = \frac{d\sigma_{\text{TMD, LO}}^{pp \rightarrow J/\psi[\Upsilon] \ell \bar{\ell} X}}{d^4q dM_B^2} \simeq \hat{F}_1^Z(Q, \alpha, \beta) C[f_1^g f_1^g]. \quad (31)$$

In a next step we evaluate the quantities  $N_Z^{(i)}$  for real Z-boson production in the hadron c.m.-frame where  $P_{a/b}^\mu = (\sqrt{S}/2)(1, 0, 0, \pm 1)$  and  $q^\mu = (\sqrt{Q^2 + \mathbf{q}_T^2} \cosh Y, \mathbf{q}_T, \sqrt{Q^2 + \mathbf{q}_T^2} \sinh Y)$ . Here,  $Y$  denotes the rapidity of quarkonium–dilepton pair, i.e., the rapidity of the final state. Also,  $d^4q = Q dQ dY d^2q_T$ . We then investigate the following distributions (ratios) that were already proposed in Ref. [27],

$$S_Z^{(0)}(Q, Y, \mathbf{q}_T) \equiv \frac{N_Z^{(0)}}{\int_0^{Q^2/4} d\mathbf{q}_T^2 N_Z^{(0)}} = \frac{C[f_1^g f_1^g]}{\int_0^{Q^2/4} d\mathbf{q}_T^2 C[f_1^g f_1^g]}, \quad (32)$$

$$S_Z^{(2)}(Q, Y, \mathbf{q}_T) \equiv \frac{N_Z^{(2)}}{\int_0^{Q^2/4} d\mathbf{q}_T^2 N_Z^{(0)}} = \frac{\hat{F}_3^Z(Q, \alpha) C[w_{3a} h_1^{\perp g} f_1^g] + C[w_{3b} f_1^g h_1^{\perp g}]}{\hat{F}_1^Z(Q, \alpha) \int_0^{Q^2/4} d\mathbf{q}_T^2 C[f_1^g f_1^g]}, \quad (33)$$

$$S_Z^{(4)}(Q, Y, \mathbf{q}_T) \equiv \frac{N_Z^{(4)}}{\int_0^{Q^2/4} d\mathbf{q}_T^2 N_Z^{(0)}} = \frac{\hat{F}_4^Z(Q, \alpha) C[w_4 h_1^{\perp g} h_1^{\perp g}]}{\hat{F}_1^Z(Q, \alpha) \int_0^{Q^2/4} d\mathbf{q}_T^2 C[f_1^g f_1^g]}. \quad (34)$$

Note that, for these ratios, the transverse momentum of the final state  $\mathbf{q}_T$  – the quarkonium–dilepton pair’s transverse momentum imbalance – is restricted to be smaller than  $Q/2$  in order to roughly fulfil the TMD factorisation requirement  $|\mathbf{q}_T| \ll Q$ .

In order to estimate the size of the effects of the linearly polarised gluons hidden in the observables  $S_Z^{(2)}$  and  $S_Z^{(4)}$ , it is instructive to first calculate the ratios of the perturbative prefactors

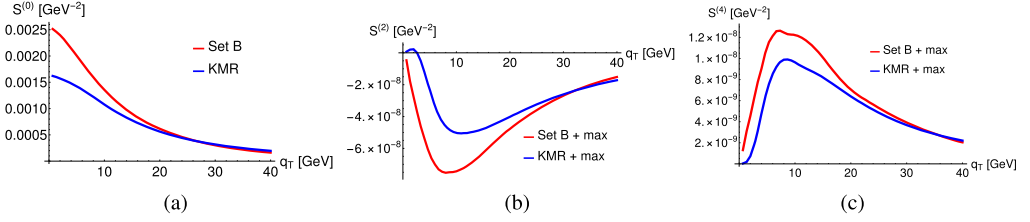


Fig. 3. The azimuthally independent distribution  $S^{(0)}$  (a) and the azimuthal distributions  $S^{(2)}$  (b) and  $S^{(4)}$  (c) at the LHC for  $\sqrt{s} = 14$  TeV for the  $\Upsilon + Z$  final state at midrapidity  $Y = 0$  and an invariant mass  $Q = 120$  GeV.

$\hat{F}_3^Z / \hat{F}_1^Z$  and  $\hat{F}_4^Z / \hat{F}_1^Z$ . We show these ratios in Fig. 2 as well, plotted vs. the invariant mass  $Q$  for a  $\Upsilon$  and  $J/\psi$  state. We find rather small ratios, around  $10^{-4}$  for  $\hat{F}_3^Z / \hat{F}_1^Z$  and  $5 \times 10^{-5}$  for  $\hat{F}_4^Z / \hat{F}_1^Z$  at the peak around  $Q = 120$  GeV for a  $\Upsilon$ -particle. The ratios for  $J/\psi$ -production are even smaller, of the order of  $10^{-6}$ . This is in contrast to the  $\Upsilon + \gamma$  final state discussed in Ref. [27] where the corresponding ratios are about 0.05 and 0.03, respectively, for an invariant mass  $Q = 20$  GeV. This already suggests that the final state containing a heavy quarkonium state and a real  $Z$ -boson may not be sufficiently suitable to study the distribution of linearly polarised gluons,  $h_1^{\perp g}$ . A more quantitative statement about the feasibility of measurements of the azimuthal observables  $S^{(2)}$  and  $S^{(4)}$  can be given through an estimate of the convolution integrals in Eqs. (32), (33), (34). We use the same model *Ansätze* for the unpolarised gluon  $f_1^g$  that were also adopted in the predictions for a  $\Upsilon + \gamma$  state in Ref. [27], where two parameterisations of the *unintegrated gluon distribution* (UGD) have been used as an input for the TMD gluon function  $f_1^g$ . Although the UGD established for small- $x$  physics may not be identified in general with the unpolarised gluon TMD, such an input serves as a first numerical estimate of the size that can be expected for the distributions  $S^{(i)}$ . In particular, we use the Set B0 solution to the CCFM equation with an initial condition based on the HERA data from Refs. [47,48] and the KMR parameterisation from Ref. [49] for the UGD. In Ref. [27] the saturation of the positivity bound [1] for the distribution of linearly polarised gluons was assumed, i.e.,  $h_1^{\perp g}(x, \mathbf{k}_T^2) = 2M^2 / \mathbf{k}_T^2 f_1^g(x, \mathbf{k}_T^2)$ . We rely on the same assumption in this work as well.

In Fig. 3 the azimuthal  $q_T$ -distribution  $S^{(2)}$  and  $S^{(4)}$  from Eqs. (33), (34) are shown for real  $Z$ -bosons and are of the size of about  $10^{-8}$ , which is about four orders of magnitudes smaller than the corresponding contributions for a  $\Upsilon + \gamma$  final state. The  $q_T$ -integrated azimuthal observables  $\int d^2q_T S^{(2)}$  and  $\int d^2q_T S^{(4)}$  amount to roughly 0.007% and 0.001%, respectively – three orders of magnitude smaller than for  $\Upsilon + \gamma$ . Hence, we conclude that it will be very difficult to access the linearly polarised gluons with a  $\Upsilon + Z$  final state. Having said that, this particular final state might be a suitable candidate for studying experimentally the unpolarised gluon TMD on its own through the measurement of the azimuthally independent distribution  $S^{(0)}$ . The difference between this observable for a  $\Upsilon + Z$  final state and a  $\Upsilon + \gamma$  final state is that the invariant mass varies. In Ref. [27] the distribution  $S^{(0)}$  was studied at  $Q = 20$  GeV for a  $\Upsilon + \gamma$  final state, while in Fig. 3 this distribution is shown for  $Q = 120$  GeV. The larger invariant mass is a consequence of the mass of the  $Z$ -boson. Hence, the  $q_T$ -distribution  $S^{(0)}$  is much broader for  $\Upsilon + Z$ . In addition, the detection of a dilepton pair at the  $Z$ -pole is experimentally much favourable in contrast to real photon detection because an isolation procedure is needed in the latter case.

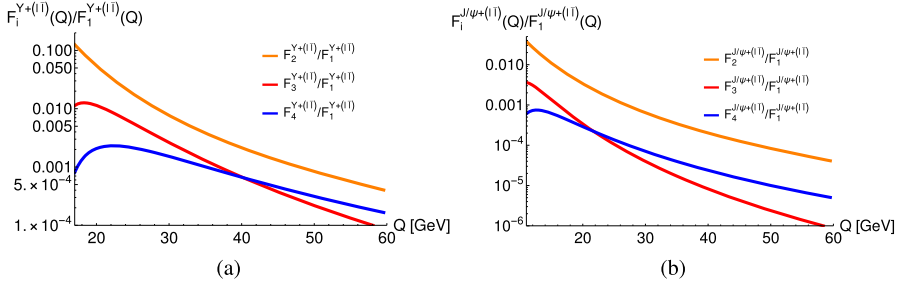


Fig. 4. The ratios  $\hat{F}_i^{\gamma\ell\bar{\ell}}(Q)/\hat{F}_1^{\gamma\ell\bar{\ell}}(Q)$  and  $\hat{F}_i^{J/\psi}(Q)/\hat{F}_1^{J/\psi}(Q)$  from (30) plotted vs. the invariant final-state mass  $Q$  for a  $\Upsilon$  (a) and a  $J/\psi$  (b). The lepton pair is selected such that only small invariant masses  $M_B \in [5 \text{ GeV}, 7 \text{ GeV}]$  are allowed.

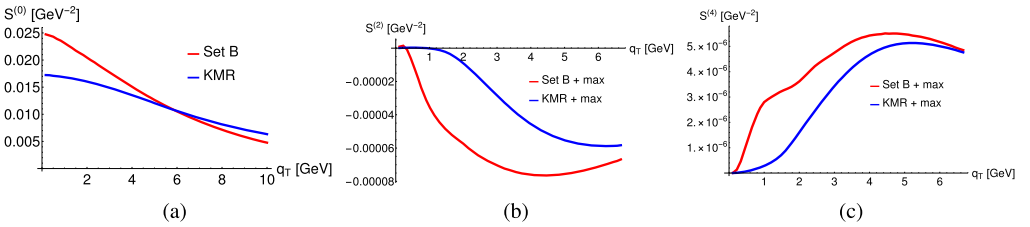


Fig. 5. The azimuthally independent distribution  $S^{(0)}$  (a) and the azimuthal distributions  $S^{(2)}$  (b) and  $S^{(4)}$  (c) for a  $\Upsilon + (\ell\bar{\ell})$  final state at midrapidity  $Y = 0$  and an invariant mass  $Q = 20 \text{ GeV}$ . The dilepton mass range is  $M_B \in [5 \text{ GeV}, 7 \text{ GeV}]$ .

#### 4. Numerical prediction for quarkonium + a dilepton from an off-shell photon

In this section we repeat the steps of the previous section but we consider lepton pairs with a relatively small invariant mass  $M_B \in [5 \text{ GeV}, 7 \text{ GeV}]$  between the  $J/\psi$  and  $\Upsilon$  families. This mass range is far away from the  $Z$ -pole mass  $m_Z$ , and dilepton creation from decays of virtual photons instead of  $Z$ -bosons should dominate.

The advantage is that we can investigate lower values of  $Q$  with a minimum final state invariant mass  $Q_{\min} = 7 \text{ GeV} + M_Q$ . In fact, we expect to observe some similarities with the associated  $Q + \gamma$  final state discussed in Ref. [27]. The theoretical formulae for this kinematic range are the same as for real  $Z$ -boson production of the last section, except that the integration region in (30) is  $5 \text{ GeV} \leq M_B \leq 7 \text{ GeV}$ .

In Fig. 4, we plot the ratios  $F_i/F_1$  for associated quarkonium–dilepton production with small dilepton masses vs. the final state invariant mass  $Q$ . We observe that these ratios are considerably larger (by 1–2 orders of magnitude) than for real  $Z$ -boson production, but still smaller than for real photon production. Overall, one can say that the associated quarkonium–dilepton final state is rather sensitive to the dilepton mass  $M_B$ . In particular, the ratio  $F_2/F_1$  indicates that the prefactor  $\hat{F}_2$  characterising the linearly polarised gluons may be a few percent of the factor  $\hat{F}_1$  for lower  $Q$ . Nevertheless, we still consider the approximation (31) to be justified.

We then calculate the  $q_T$ -distributions  $S^{(i)}$  for small dilepton masses and show our results in Fig. 5. Since the distribution  $S^{(0)}$  in the upper panel does not depend on the specific final state, we obtain the same result for a final state invariant mass  $Q = 20 \text{ GeV}$  as for real photon production in Ref. [27]. The ratios  $F_{3,4}/F_1$  are smaller compared to real photon production as mentioned before, and this results in smaller azimuthal  $q_T$ -distributions  $S^{(2)}$  and  $S^{(4)}$ . We estimate the

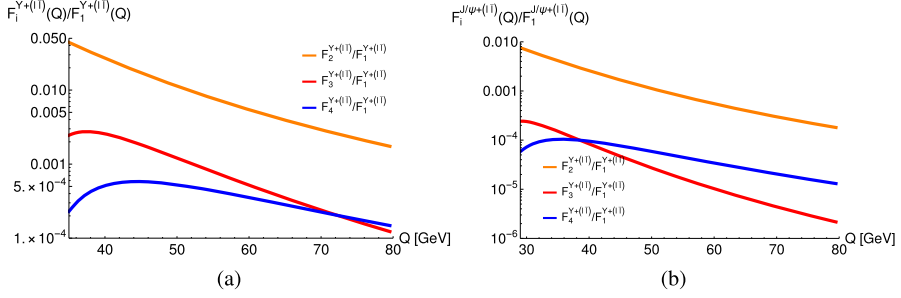


Fig. 6. Same as Fig. 4, but in the dilepton mass range  $M_B \in [20 \text{ GeV}, 25 \text{ GeV}]$ .

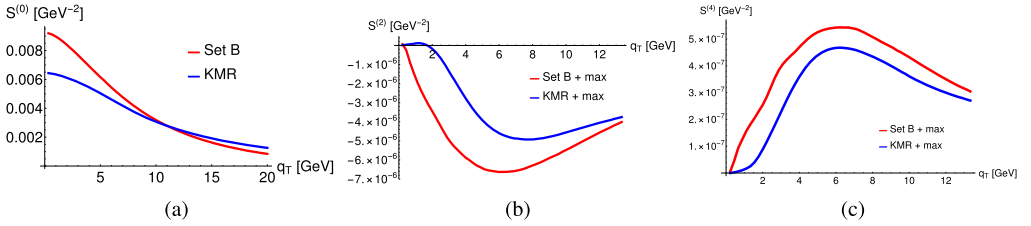


Fig. 7. Same as Fig. 5, but in the dilepton mass range  $M_B \in [20 \text{ GeV}, 25 \text{ GeV}]$ .

overall  $q_T$ -integrated  $\cos 2\phi$  effect from linearly polarised gluons to be about 0.5%–0.6% in the dilepton mass range  $M_B \in [5 \text{ GeV}, 7 \text{ GeV}]$  for an invariant mass  $Q = 20 \text{ GeV}$ , while the  $\cos 4\phi$  modulation amounts to 0.04%–0.045%. Although these rates are smaller by an order of magnitude compared to real photon production, the experimental advantage of cleaner final state may outweigh the disadvantage of a smaller effect. This discussion is however beyond the scope of the present analysis.

Finally, we also investigate an intermediate dilepton mass range  $M_B \in [20 \text{ GeV}, 25 \text{ GeV}]$ . The corresponding ratios of the LO prefactors  $F_i/F_1$  are shown in Fig. 6 where we observe a reduction of a factor of about 3–4 compared to the small dilepton mass range  $M_B \in [5 \text{ GeV}, 7 \text{ GeV}]$ , both for a  $\Upsilon$  and  $J/\psi$ . Consequently, also the azimuthal  $q_T$ -distributions  $S^{(2)}$  and  $S^{(4)}$ , taken at a larger invariant final state mass  $Q = 40 \text{ GeV}$  and shown in Fig. 7, are smaller. The overall effect amounts to 0.13%–0.15% for the  $\cos 2\phi$  modulation and 0.01%–0.012% for the  $\cos 4\phi$  modulation.

### 5. Conclusions

In this paper, we have presented the treatment of an arbitrary process induced by gluon–gluon fusion with a colour-singlet final state in the TMD approach. Using the helicity formalism, we have analysed the general structure of the fully differential, unpolarised cross section for this process in terms of TMD distributions of unpolarised and linearly polarised gluons inside an unpolarised nucleon. We have then calculated the partonic cross sections underlying the azimuthally independent and dependent structures of the hadronic cross section for a specific final state: a heavy quarkonium in a colour-singlet state and a real  $Z$ -boson. We have found that, in contrast to quarkonium production associated with a photon, the azimuthally dependent contributions are strongly suppressed with respect to the azimuthally independent ones. Therefore, the distribution of linearly polarised gluons in the nucleon is most probably not experimentally accessible for a

quarkonium final state that is associated with a real  $Z$ -boson. The unpolarised gluon TMDs may however be studied by means of the azimuthally independent transverse momentum distribution of the process  $pp \rightarrow \Upsilon ZX$ , which can be directly measured at the LHC.

We have also investigated the associated quarkonium + dilepton production for small and medium dilepton masses. These dileptons are predominantly generated from virtual photon decays. Although the effects from linearly polarised gluons are still smaller than for the real-photon case, a TMD extraction might be done for dilepton masses between the  $J/\psi$  and  $\Upsilon$  masses at the LHC in view of the recent experimental studies of  $\Upsilon + \Upsilon$  [50] and  $J/\psi + \Upsilon$  [51] production.

## Acknowledgements

We thank D. Boer, W. den Dunnen, M.G. Echevarria, T. Kasemets, H.S. Shao, A. Signori, J.X. Wang for helpful discussions. The work of C.P. is supported by the European Research Council (ERC) under the European Union’s Horizon 2020 research and innovation programme (grant agreement No. 647981, 3DSPIN). The work of J.P.L. is supported in part by the CNRS-IN2P3 (project TMD@NLO). The work of M.S. is supported in part by the Bundesministerium für Bildung und Forschung (BMBF) grant 05P15VTCA1.

## References

- [1] P.J. Mulders, J. Rodrigues, Transverse momentum dependence in gluon distribution and fragmentation functions, *Phys. Rev. D* 63 (2001) 094021, arXiv:hep-ph/0009343.
- [2] D. Boer, C. Lorcé, C. Pisano, J. Zhou, The gluon Sivers distribution: status and future prospects, *Adv. High Energy Phys.* 2015 (2015) 371396, arXiv:1504.04332 [hep-ph].
- [3] J. Collins, *Foundations of Perturbative QCD*, Cambridge University Press, 2013, <http://www.cambridge.org/de/knowledge/isbn/item5756723>.
- [4] S.M. Aybat, T.C. Rogers, TMD parton distribution and fragmentation functions with QCD evolution, *Phys. Rev. D* 83 (2011) 114042, arXiv:1101.5057 [hep-ph].
- [5] M.G. Echevarria, A. Idilbi, I. Scimemi, Factorization theorem for Drell–Yan at low  $q_T$  and transverse momentum distributions on-the-light-cone, *J. High Energy Phys.* 07 (2012) 002, arXiv:1111.4996 [hep-ph].
- [6] J.P. Ma, J.X. Wang, S. Zhao, Transverse momentum dependent factorization for quarkonium production at low transverse momentum, *Phys. Rev. D* 88 (1) (2013) 014027, arXiv:1211.7144 [hep-ph].
- [7] P. Sun, B.-W. Xiao, F. Yuan, Gluon distribution functions and Higgs boson production at moderate transverse momentum, *Phys. Rev. D* 84 (2011) 094005, arXiv:1109.1354 [hep-ph].
- [8] D. Boer, W.J. den Dunnen, TMD evolution and the Higgs transverse momentum distribution, *Nucl. Phys. B* 886 (2014) 421–435, arXiv:1404.6753 [hep-ph].
- [9] M.G. Echevarria, T. Kasemets, P.J. Mulders, C. Pisano, QCD evolution of (un)polarized gluon TMDPDFs and the Higgs  $q_T$ -distribution, *J. High Energy Phys.* 07 (2015) 158, arXiv:1502.05354 [hep-ph].
- [10] M.G. Echevarria, A. Idilbi, A. Schäfer, I. Scimemi, Model-independent evolution of transverse momentum dependent distribution functions (TMDs) at NNLL, *Eur. Phys. J. C* 73 (12) (2013) 2636, arXiv:1208.1281 [hep-ph].
- [11] D. Boer, S.J. Brodsky, P.J. Mulders, C. Pisano, Direct probes of linearly polarized gluons inside unpolarized hadrons, *Phys. Rev. Lett.* 106 (2011) 132001, arXiv:1011.4225 [hep-ph].
- [12] C. Pisano, D. Boer, S.J. Brodsky, M.G.A. Buffing, P.J. Mulders, Linear polarization of gluons and photons in unpolarized collider experiments, *J. High Energy Phys.* 10 (2013) 024, arXiv:1307.3417 [hep-ph].
- [13] D. Boer, P.J. Mulders, C. Pisano, J. Zhou, Asymmetries in heavy quark pair and dijet production at an EIC, *J. High Energy Phys.* 08 (2016) 001, arXiv:1605.07934 [hep-ph].
- [14] J.-W. Qiu, M. Schlegel, W. Vogelsang, Probing gluonic spin-orbit correlations in photon pair production, *Phys. Rev. Lett.* 107 (2011) 062001, arXiv:1103.3861 [hep-ph].
- [15] D. Boer, C. Pisano, Polarized gluon studies with charmonium and bottomonium at LHCb and AFTER, *Phys. Rev. D* 86 (2012) 094007, arXiv:1208.3642 [hep-ph].
- [16] J.P. Lansberg, et al., Spin physics and TMD studies at A Fixed-Target Experiment at the LHC (AFTER@LHC), *EPJ Web Conf.* 85 (2015) 02038, arXiv:1410.1962 [hep-ex].

- [17] R. Angeles-Martinez, et al., Transverse momentum dependent (TMD) parton distribution functions: status and prospects, *Acta Phys. Pol. B* 46 (12) (2015) 2501–2534, arXiv:1507.05267 [hep-ph].
- [18] J.P. Lansberg, Back-to-back isolated photon–quarkonium production at the LHC and the transverse-momentum-dependent distributions of the gluons in the proton, *Int. J. Mod. Phys. Conf. Ser.* 40 (2016) 1660015, arXiv:1502.02263 [hep-ph].
- [19] A. Signori, Gluon TMDs in quarkonium production, *Few-Body Syst.* 57 (8) (2016) 651–655, arXiv:1602.03405 [hep-ph].
- [20] A. Signori, Flavor and Evolution Effects in TMD Phenomenology, PhD thesis, Vrije U., Amsterdam, 2016, <http://inspirehep.net/record/1493030/files/Thesis-2016-Signori.pdf>.
- [21] D. Boer, Gluon TMDs in quarkonium production, *Few-Body Syst.* 58 (2) (2017) 32, arXiv:1611.06089 [hep-ph].
- [22] J.P. Ma, J.X. Wang, S. Zhao, Breakdown of QCD factorization for P-wave quarkonium production at low transverse momentum, *Phys. Lett. B* 737 (2014) 103–108, arXiv:1405.3373 [hep-ph].
- [23] A. Andronic, et al., Heavy-flavour and quarkonium production in the LHC era: from proton–proton to heavy-ion collisions, *Eur. Phys. J. C* 76 (3) (2016) 107, arXiv:1506.03981 [nucl-ex].
- [24] N. Brambilla, et al., Heavy quarkonium: progress, puzzles, and opportunities, *Eur. Phys. J. C* 71 (2011) 1534, arXiv:1010.5827 [hep-ph].
- [25] J.P. Lansberg,  $J/\psi$ ,  $\psi'$  and  $\Upsilon$  production at hadron colliders: a review, *Int. J. Mod. Phys. A* 21 (2006) 3857–3916, arXiv:hep-ph/0602091.
- [26] LHCb Collaboration, R. Aaij, et al., Measurement of the  $\eta_c(1S)$  production cross-section in proton–proton collisions via the decay  $\eta_c(1S) \rightarrow p\bar{p}$ , *Eur. Phys. J. C* 75 (7) (2015) 311, arXiv:1409.3612 [hep-ex].
- [27] W.J. den Dunnen, J.P. Lansberg, C. Pisano, M. Schlegel, Accessing the transverse dynamics and polarization of gluons inside the proton at the LHC, *Phys. Rev. Lett.* 112 (2014) 212001, arXiv:1401.7611 [hep-ph].
- [28] D. Boer, C. Pisano, Impact of gluon polarization on Higgs boson plus jet production at the LHC, *Phys. Rev. D* 91 (7) (2015) 074024, arXiv:1412.5556 [hep-ph].
- [29] D. Boer, W.J. den Dunnen, C. Pisano, M. Schlegel, W. Vogelsang, Linearly polarized gluons and the Higgs transverse momentum distribution, *Phys. Rev. Lett.* 108 (2012) 032002, arXiv:1109.1444 [hep-ph].
- [30] D. Boer, W.J. den Dunnen, C. Pisano, M. Schlegel, Determining the Higgs spin and parity in the diphoton decay channel, *Phys. Rev. Lett.* 111 (3) (2013) 032002, arXiv:1304.2654 [hep-ph].
- [31] ATLAS Collaboration, G. Aad, et al., Observation and measurements of the production of prompt and non-prompt  $J/\psi$  mesons in association with a Z boson in  $pp$  collisions at  $\sqrt{s} = 8$  TeV with the ATLAS detector, *Eur. Phys. J. C* 75 (5) (2015) 229, arXiv:1412.6428 [hep-ex].
- [32] J.-P. Lansberg, H.-S. Shao, Associated production of a quarkonium and a Z boson at one loop in a quark–hadron-duality approach, *J. High Energy Phys.* 10 (2016) 153, arXiv:1608.03198 [hep-ph].
- [33] B. Gong, J.-P. Lansberg, C. Lorce, J. Wang, Next-to-leading-order QCD corrections to the yields and polarisations of  $J/\psi$  and Upsilon directly produced in association with a Z boson at the LHC, *J. High Energy Phys.* 03 (2013) 115, arXiv:1210.2430 [hep-ph].
- [34] S. Mao, M. Wen-Gan, L. Gang, Z. Ren-You, G. Lei, QCD corrections to  $J/\psi$  plus  $Z^0$ -boson production at the LHC, *J. High Energy Phys.* 02 (2011) 071, arXiv:1102.0398 [hep-ph];  
S. Mao, M. Wen-Gan, L. Gang, Z. Ren-You, G. Lei, *J. High Energy Phys.* 12 (2012) 010 (Erratum).
- [35] ATLAS Collaboration, G. Aad, et al., Search for Higgs and Z boson decays to  $J/\psi\gamma$  and  $\Upsilon(nS)\gamma$  with the ATLAS detector, *Phys. Rev. Lett.* 114 (12) (2015) 121801, arXiv:1501.03276 [hep-ex].
- [36] R. Li, J.-X. Wang, Next-to-leading-order QCD corrections to  $J/\psi(\nu) + \gamma$  production at the LHC, *Phys. Lett. B* 672 (2009) 51–55, arXiv:0811.0963 [hep-ph].
- [37] J.P. Lansberg, Real next-to-next-to-leading-order QCD corrections to  $J/\psi$  and Upsilon hadroproduction in association with a photon, *Phys. Lett. B* 679 (2009) 340–346, arXiv:0901.4777 [hep-ph].
- [38] ATLAS Collaboration, G. Aad, et al., Measurement of the production cross section of prompt  $J/\psi$  mesons in association with a  $W^\pm$  boson in  $pp$  collisions at  $\sqrt{s} = 7$  TeV with the ATLAS detector, *J. High Energy Phys.* 04 (2014) 172, arXiv:1401.2831 [hep-ex].
- [39] J.P. Lansberg, C. Lorce, Reassessing the importance of the colour-singlet contributions to direct  $J/\psi + W$  production at the LHC and the Tevatron, *Phys. Lett. B* 726 (2013) 218–222, arXiv:1303.5327 [hep-ph];  
J.P. Lansberg, C. Lorce, *Phys. Lett. B* 738 (2014) 529 (Erratum).
- [40] G. Li, M. Song, R.-Y. Zhang, W.-G. Ma, QCD corrections to  $J/\psi$  production in association with a W-boson at the LHC, *Phys. Rev. D* 83 (2011) 014001, arXiv:1012.3798 [hep-ph].
- [41] S. Meissner, A. Metz, K. Goeke, Relations between generalized and transverse momentum dependent parton distributions, *Phys. Rev. D* 76 (2007) 034002, arXiv:hep-ph/0703176.
- [42] P. Sun, C.P. Yuan, F. Yuan, Kinematical correlations for Higgs boson plus high  $P_t$  jet production at hadron colliders, *Phys. Rev. Lett.* 114 (20) (2015) 202001, arXiv:1409.4121 [hep-ph].

- [43] P. Sun, J. Isaacson, C.P. Yuan, F. Yuan, Resummation of high order corrections in higgs boson plus jet production at the LHC, arXiv:1602.08133 [hep-ph].
- [44] C.H. Kom, A. Kulesza, W.J. Stirling, Pair production of  $J/\psi$  as a probe of double parton scattering at LHCb, Phys. Rev. Lett. 107 (2011) 082002, arXiv:1105.4186 [hep-ph].
- [45] J.-P. Lansberg, H.-S. Shao,  $J/\psi$ -pair production at large momenta: indications for double parton scatterings and large  $\alpha_s^5$  contributions, Phys. Lett. B 751 (2015) 479–486, arXiv:1410.8822 [hep-ph].
- [46] J.-P. Lansberg, H.-S. Shao, Phenomenological analysis of associated production of  $Z^0 + b$  in the  $b \rightarrow J/\psi X$  decay channel at the LHC, Nucl. Phys. B 916 (2017) 132–142, arXiv:1611.09303 [hep-ph].
- [47] H. Jung, Un-integrated PDFs in CCFM, in: Proceedings, 12th International Workshop on Deep Inelastic Scattering (DIS 2004): Strbske Pleso, Slovakia, April 14–18, 2004, 2004, pp. 299–302, arXiv:hep-ph/0411287, <http://www.saske.sk/dis04/proceedings/A/jungA.ps.gz>.
- [48] H. Jung, et al., The CCFM Monte Carlo generator CASCADE version 2.2.03, Eur. Phys. J. C 70 (2010) 1237–1249, arXiv:1008.0152 [hep-ph].
- [49] M.A. Kimber, A.D. Martin, M.G. Ryskin, Unintegrated parton distributions, Phys. Rev. D 63 (2001) 114027, arXiv:hep-ph/0101348.
- [50] CMS Collaboration, V. Khachatryan, et al., Observation of  $\Upsilon(1S)$  pair production in proton–proton collisions at  $\sqrt{s} = 8$  TeV, J. High Energy Phys. (2016), submitted for publication, arXiv:1610.07095 [hep-ex].
- [51] D0 Collaboration, V.M. Abazov, et al., Evidence for simultaneous production of  $J/\psi$  and  $\Upsilon$  mesons, Phys. Rev. Lett. 116 (8) (2016) 082002, arXiv:1511.02428 [hep-ex].